ACS APPLIED MATERIALS & INTERFACES

Research Article

www.acsami.org

Tailoring Highly Oriented and Micropatterned Clay/Polymer Nanocomposites by Applying an a.c. Electric Field

Erwan Paineau,*[,†] Ivan Dozov,[†] Isabelle Bihannic,[‡] Christophe Baravian,[§] Marie-Eve M. Krapf,[‡,⊥] Adrian-Marie Philippe,[§] Stéphan Rouzière,[†] Laurent J. Michot,[‡] and Patrick Davidson[†]

[†]Laboratoire de Physique des Solides, UMR 8502, Paris-Sud University, Bâtiment 510, 91405 Orsay Cedex, France

[‡]Laboratoire Environnement et Minéralurgie, UMR 7569, Nancy University, BP 40, 54501 Vandoeuvre Cedex, France

[§]Laboratoire d'Energétique et de Mécanique Théorique et Appliquée, UMR 7563, Nancy University, BP 160, 54504 Vandoeuvre Cedex, France

ABSTRACT: Clay/polymer nanocomposites have recently raised much interest because of their widespread industrial applications. Nevertheless, controlling both clay platelet exfoliation and orientation during polymerization still remains challenging. Herein, we report the elaboration of clay/polymer nanocomposite hydrogels from aqueous suspensions of natural swelling clays submitted to high-frequency a.c. electric fields. X-ray scattering experiments have confirmed the complete exfoliation of the clay sheets in the polymer matrix, even after polymerization. Moreover, polarized light microscopy shows that the clay platelets were perfectly oriented by the electric field and that this field-induced alignment was frozen in by in situ photopolymerization. This procedure allowed us to not only produce uniformly aligned samples but also pattern platelet orientation, at length scales down to 20 μm. This straightforward and cheap nanocomposite patterning technique can be easily extended to a wide range of natural or synthetic inorganic anisotropic particles.

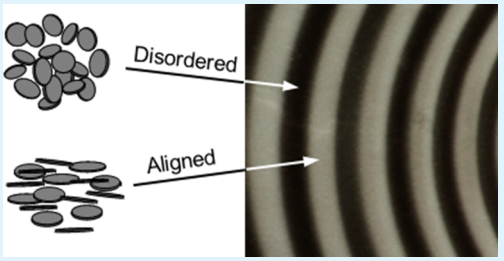

KEYWORDS: *clay, composite, electric field, exfoliation, alignment*

1. INTRODUCTION

Since the synthesis of nylon 6-clay hybrid materials by Toyota engineers in 1993,[1] a wide range of new clay/polymer nanocomposites has emerged, as illustrated by numerous reviews.[2−5] Clay minerals have attracted much attention due to their high aspect ratio, unique colloidal properties (thixotropy, viscoelasticity, yield stress), low cost, and environmental friendliness. The addition of these layered minerals drastically enhances the properties of the polymer materials. Indeed, polymeric hydrogels, prepared by hybridization of polymers with small amounts of swelling clays, have shown superior mechanical, optical, and gas-barrier properties compared to conventional polymer composites.[6−9] As recently reported, novel clay-filled hydrogels can even display exceptional self-healing behavior.[10] The outstanding features of clay−polymer nanocomposites are closely linked to the degree of clay sheet exfoliation and orientation in the polymer matrix. For this reason, various synthesis routes have been explored to achieve complete clay exfoliation in polymer nanocomposites.[4] Still, controlling platelet orientation during polymerization remains challenging. For this purpose, several groups have used sample shearing to align clay/polymer nanocomposites. Investigations of the organization of the clay platelets using either Small-Angle Neutron Scattering (SANS),[11,12] transmission electron microscopy (TEM),[13] or optical birefringence[14] revealed, in most cases, fairly good alignment. However, some particles remain aggregated, which hampers their alignment. Meanwhile, Vaia et al.[15] proposed an alternative approach using holographic photopolymerization. This one-step technique allows the formation of one-dimensional gratings with submicrometer resolution although clay particles are segregated in the resulting material and they are not oriented. A more efficient way of controlling orientation in clay/polymer nanocomposites could be to apply an electric or a magnetic field, as classically done with liquid crystals.[16,17] Only few experiments explored this route so far.[18,19] Even though significant improvement of orientation was thus obtained, complete exfoliation was not achieved as the field-induced structure was made up of small aligned stacks of about ten particles rather than individual platelets homogeneously oriented in the final nanocomposite.

We recently investigated the phase diagram of size-selected, natural beidellite particles, proving the existence of an isotropic/nematic phase transition at low volume fraction.[20] In the liquid-crystalline nematic phase, the clay platelets are aligned in the same direction (called the nematic director **n**) in contrast to the isotropic phase that shows no orientational order of the platelets. Small-Angle X-ray Scattering (SAXS) experiments revealed that the aqueous colloidal suspensions of the smallest size fractions (average sheet diameter $D \approx 200$

Received: June 1, 2012
Accepted: July 25, 2012
Published: July 25, 2012

nm) are only composed of individual clay platelets, with an average thickness of 0.7 nm.[21] Electric and magnetic fields were used to produce single domains of the nematic phase, with a very large nematic order parameter $S_2 \approx 0.8$, which underlines the quite good alignment of the platelets.[20] Furthermore, the electric field induces perfect "anti-nematic" order ($S_2 = -0.5$) in isotropic suspensions.[22] Indeed, the clay sheets align their normal perpendicular to the electric field, resulting in a uniaxial orientational order different from the usual nematic one as the platelet symmetry axis aligns perpendicular to the director rather than parallel to it. The orientation mechanism of the clay particles in an alternating electric field proceeds from the anisotropy of the strong induced polarization of the electric double layer of counterions at the charged particle/electrolyte interface.

Taking advantage of these properties of beidellite suspensions, we report here a straightforward approach, by applying a.c. electric fields, to control and tailor perfectly exfoliated and oriented clay/polymer nanocomposites and to micropattern platelet orientation. We chose a photopolymerization process with acrylamide monomers and *N,N′*-methylenebisacrylamide cross-linkers. This approach avoids any organic treatment of clay particles and allows triggering polymerization by simply using light. Furthermore, using such fast polymerization process, the clay alignment can be frozen after removing the electric field.

2. EXPERIMENTAL SECTION

2.1. Clay Preparation. Natural beidellite SBId-1 (Idaho) was purchased from the Source Clays Minerals Repository (Purdue University, USA). The structural formula of beidellite was defined from chemical analyses by Post et al.[23] as $(Si_{7.27}Al_{0.73})$-$(Al_{3.77}Fe^{3+}_{0.11}Mg_{0.21})O_{20}(OH)_4(Na,Ca)_{0.67}$. Prior to use, raw samples were purified and homoionized under their lithium form, followed by a size-fractionation step to reduce polydispersity.[20] The particles used here have average diameter of 200 nm (polydispersity $\sigma_D = 37\%$) and thickness of 0.7 nm.[21] A dilute stock suspension (~10 g L^{-1}) was then concentrated in Milli-Q water by osmotic stress to a volume fraction ϕ of 0.8% by using regenerated cellulose dialysis tubes (Visking, MWCO = 14 00 Da, Roth) and polyethyleneglycol solutions (PEG 20000, 20 g L^{-1}, Carl Roth GmbH).[20]

2.2. Synthesis. Following the synthesis route applied previously with α-chitin suspensions,[24] swollen polymer gels were prepared from a 40% solution of acrylamide and *N,N′*-methylenebisacrylamide monomers (mixing ratio 29:1, Carl Roth GmbH). In-situ photopolymerization was initiated by Riboflavin (5×10^{-4} M, Sigma) and catalyzed by *N,N,N′,N′*-tetramethylethylenediamine (1.5×10^{-3} M, Sigma). This solution was mixed with aliquots (1 mL) of concentrated clay suspensions to reach final volume fractions ranging from $\phi = 0.3-0.5\%$, the isotropic/nematic transition being located from $\phi = 0.42\%$ for this size fraction.[20] This procedure requires no additional organic treatment of clay particles since the monomer, cross-linker, catalyst, and initiator are all water-soluble. The suspensions obtained were introduced into either borosilicate flat rectangular (sample thickness, $d = 0.2$ mm; sample width $w = 2$ mm, VitroCom) or cylindrical (1 mm, GLAS) capillaries and stored vertically after flame-sealing.

2.3. Measurements. Optical observations and birefringence (Δn) measurements were carried out with a polarizing microscope (Eclipse LV100pol, Nikon) equipped with a CCD camera and a Berek compensator inserted at 45° with respect to both polarizer and analyzer directions. X-ray scattering experiments were performed using a rotating anode generator ($\lambda_{CuK\alpha} = 0.154$ nm, Rigaku) and a multilayer W/Si optics (Osmic). The sample to detector distance was 425 mm. Scattering patterns were collected on a Mar345 image plate detector with 150 μm pixel size. Curves of scattered intensity versus scattering vector modulus q ($q = 4\pi\sin\theta/\lambda$, where 2θ is the scattering angle) were deduced from azimuthal angular integration of the patterns previously corrected for water, glass, and kapton scattering. The electro-optic setup was fully described previously.[22] Briefly, the sample holder was placed on the stage of a polarizing microscope (Leitz Ortholux) equipped with a 100 W tungsten-filament lamp. The electric field was applied using external aluminum foil electrodes, fixed at the capillary wall (4.5 mm apart). High-frequency (700 kHz) sinusoidal a.c. voltage (200 V), either continuous or pulsed, was applied to the electrodes using a pulse generator, two function generators synthesizing the high-frequency sinusoidal field and the envelope shape, respectively, an amplitude modulator mixing these two signals, and a fast amplifier (Krohn-Hite 7602M). The electric field E penetrating in the sample is parallel to the capillary long axis, highly uniform (less than 3% variation), and can be estimated around 20 V/mm.[22] The microscope is equipped with a Berek compensator and with a photomultiplier tube detector, enabling in situ measurement of the field-induced birefringence before, during and after the polymerization of the samples.

3. RESULTS AND DISCUSSION

We first checked that monomer addition does not affect exfoliation by performing X-ray scattering measurements on doped suspensions (i.e., containing the clay platelets, monomers, cross-linkers, catalyst, and photoinitiators). Typical X-ray scattering curves obtained on pure and doped clay suspensions (Figure 1a,b) are quite similar: at small angles, the

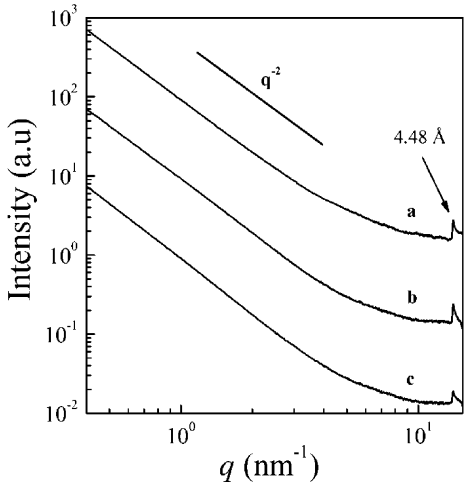

Figure 1. X-ray scattering data for pure (a), doped (i.e., containing the clay platelets, monomers, cross-linkers, catalyst, and photoinitiators) (b), and polymerized (c) beidellite suspensions ($\phi = 0.4\%$. The arrow indicates the d*(02-, 11-)* Bragg peak arising from the sheet crystalline structure.

scattering intensity decreases monotonously with the scattering vector modulus q, as q^{-2}, which confirms the bidimensional nature of isolated scattering objects.[20,21] At wide angles, a sharp asymmetric peak, at $q \approx 14$ nm^{-1}, is the only feature observed and is assigned to the typical $d(20-;11-)$ Bragg peak of the clay sheet structure. The absence of any $d(001)$ peak proves that no aggregation occurs in the presence of monomers and that the clay exfoliation is complete. After polymerization (Figure 1c), the scattering pattern is not modified, which clearly reveals that this process does not induce any aggregation either. Therefore, the clay−polymer composites are based only on single clay sheets.

The liquid-crystalline properties of pure and doped suspensions were analyzed by polarized optical microscopy (POM). Like pure beidellite suspensions, freshly prepared doped suspensions display, after a few hours, the nucleation and

coalescence of birefringent droplets, followed by a phase separation between an upper isotropic phase and a birefringent nematic one (Figure 2a).[20] As already observed in pure

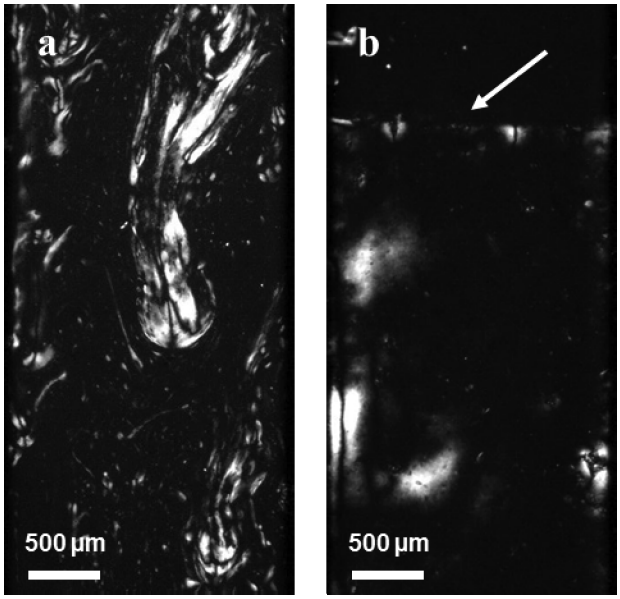

Figure 2. Polarized optical microscope (POM) images between crossed polarizers of a biphasic sample (ϕ = 0.5%) of a doped suspension in a flat glass capillary (a) 1 h and (b) 1 week after homogenization. The white arrow points to the (barely visible) meniscus between the upper isotropic phase and the bottom nematic phase in homeotropic anchoring.

suspensions, the nematic texture presents large dark areas (Figure 2b) that actually are homeotropic domains (i.e., with the nematic director parallel to the light beam) revealing the orientation of clay platelets parallel to the surface of the flat glass walls.[20] All these features confirm that the addition of monomer, cross-linker, catalyst, and photoinitiator does not significantly alter the physical properties of the clay platelet suspensions.

Sample polymerization was first performed in the absence of any electric field. The sample was placed on a polarizing microscope stage and polymerized in situ, using the light from the microscope lamp, focused on the capillary. Polymerization is activated by both the near-UV light emitted by the lamp and the heating of the sample due to light absorption. Using this procedure, polymerization can be triggered in selected, well-defined areas of the sample. Indeed, polymerization starts at the most strongly illuminated place, usually at the center of the field of view, and then propagates away from it. A sharp polymerization front advances rapidly in the liquid suspension, leaving behind a uniform composite material. Adjusting light intensity and temperature provides an efficient control of the propagation speed (up to 1 mm s^{-1}) of the polymerization front. Locally, the polymerization process is quite fast as could be estimated by examining the transient birefringence response of the sample to very short electric field square pulses with a photomultiplier tube.[22] Indeed, in about 100 ms after passage of the polymerization front, the composite is gelled, effectively blocking the rotational and translational diffusion of the clay particles whose initial orientation is frozen. Consequently, starting from the isotropic phase, an isotropic composite material is obtained. Accordingly, if the particles are previously oriented in the suspension, e.g. by applying an electric field, an oriented composite material can be produced, with potentially anisotropic optical, electrical, mechanical, and transport properties. Below, we focus on the influence of an a.c. electric field on isotropic suspensions (ϕ = 0.4%) rather than nematic ones for several reasons: (i) this avoids all problems related to surface anchoring of the nematic director (ii) a very strong orientational order ($S \approx -0.5$) can be readily obtained at moderate voltages[22] (iii) the low viscosity of the isotropic phase[25] ensures fast response times, which allows micropatterning platelet orientation in the samples. Moreover, higher clay volume fractions always lead to the physical gelation of the suspensions,[25] which effectively prevents any effect of the electric field on particle orientation.

The liquid suspensions were aligned by applying a uniform electric field along the capillary axis, using a pair of external electrodes. This technique avoids any sample degradation by electrolysis and provides a precise control of the region where alignment takes place. As already reported, this experimental setup allows inducing a strong antinematic order in isotropic suspensions of disk-like particles.[22] The orientational order was monitored by in situ optical observation of the sample as polymerization proceeds.

A constant voltage was first applied to the electrodes during polymerization and the whole interelectrode area was illuminated. As expected, the particles are oriented by the electric field, resulting in a field-dependent phase shift, $\Delta L(E) = d\Delta n(E)$ (this shift is actually the optical path difference of ordinary and extraordinary light rays arising from the optical anisotropy of the sample). Before polymerization, the phase-shift varies with the field and follows any steplike change with the usual short relaxation time (~10 ms) typical for the isotropic liquid suspension. In contrast, behind the traveling polymerization front, the phase-shift does not follow any field variation, confirming that particle reorientation is effectively blocked by the gelled polymer matrix (Figure 3a).

The curves of phase-shift versus applied voltage, measured before and after polymerization, are close to each other (Figure 3b), confirming that the electric-field-induced order is not modified upon polymerization. The phase-shift is even slightly larger after polymerization, probably due to some additional birefringence of the polymerized sample due to anisotropic mechanical stresses frozen within the sample by the polymerization process. The induced orientational order parameter S_2, related to the average orientation of the particle axis ($S_2 = (1/2)\langle 3\cos^2\theta - 1\rangle$, where θ is the angle between the clay platelet normal and the nematic director $\mathbf{n}$) was directly deduced from the saturated values of the birefringence,[22] $S_2 = \Delta n^{sat}/(\phi \Delta n^P)$, where Δn^P is the specific average optical anisotropy, i.e., when the birefringence is extrapolated to ϕ = 1 and for a perfectly oriented system (S_2 = 1). Using the value of $\Delta n^P = -0.09$ deduced previously,[22] the order parameter of the oriented sample at saturation is $S_2 = -0.44$, close to the theoretical limit $S^{sat} = -1/2$ for a perfectly oriented antinematic phase.

This almost perfect field-induced-alignment of the clay platelets should have a very significant impact on the physical properties of these nanocomposite materials. Indeed, all their mechanical properties, such as Young modulus or tensile strength for instance, should be very anisotropic. Moreover, all barrier and transport properties, like permeability, strongly depend on the tortuosity coefficient that is a function of both particle aspect ratio and nematic order parameter.[4,26,27] The possibility to apply the electric field in any desired direction

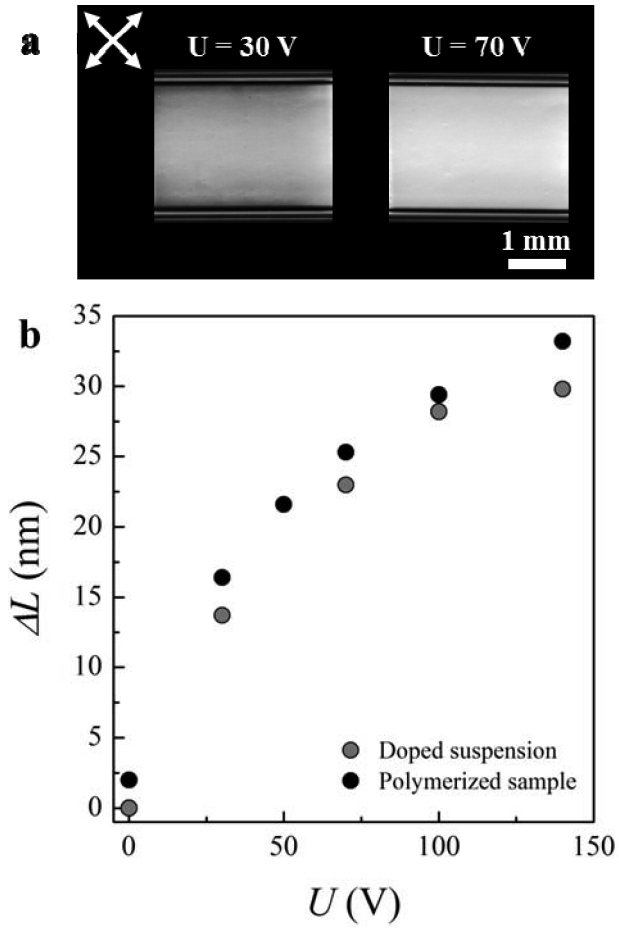

Figure 3. (a) POM images between crossed polarizers (white arrows) of the field-induced birefringence of samples polymerized at different voltages; (b) phase-shift measures before (gray) and after (black) polymerization, as a function of the voltage applied during the polymerization. The clay volume fraction is ϕ = 0.4%.

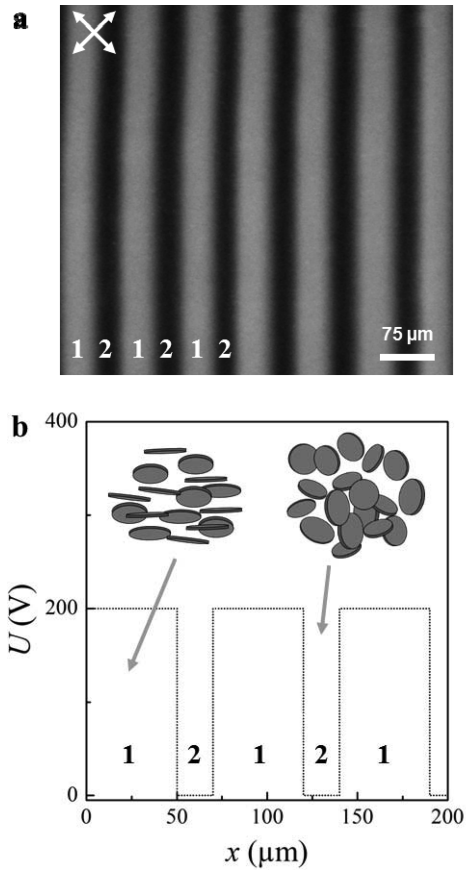

Figure 4. (a) POM image between crossed polarizers (white arrows) of a composite sample (ϕ = 0.4%) patterned with a step-like modulation. (b) Corresponding applied a.c. voltage amplitude at the position of the traveling polymerization front. The sketches represent either the (1) antinematic or (2) isotropic platelet organization.

with respect to the sample geometry provides an additional advantage over other traditional alignment techniques such as mechanical-shear alignment. Further investigations are clearly needed at this stage in order to demonstrate any improvement in these properties.

Composite samples, with anisotropy patterned in one dimension, can be easily produced thanks to the fast and localized traveling polymerization front. As an illustration of this idea, we placed in the microscope light path a rectangular mask, shading half the field of view. The mask is placed before the condenser lens, in a plane optically conjugate to the image plane, casting a sharp shadow on the sample. At the start of the experiment, the border of the mask shade is set close to one electrode, only leaving a narrow band exposed to the light. The polymerization front, parallel to the mask border, starts traveling away from the electrode. Upon a continuous displacement of the mask toward the other electrode, the sample is progressively exposed to both UV-light and heat from the lamp and the polymerization front follows the mask displacement with a small delay. Meanwhile, the voltage amplitude is sharply modulated in time, which in turn also modulates the orientational order induced in the liquid phase ahead of the polymerization front (Figure 4a,b).

At the traveling interface, where polymerization takes place, the particles are blocked in their instantaneous field-induced orientation. Consequently, the patterned composite material exhibits a step-like sequence of isotropic and aligned bands separated by fairly sharp interfaces (Figure 4a). The period of this modulation is here around 50 μm and remains quite constant. It could simply be tuned by carefully adjusting the mask displacement speed.

In addition, the shape of the patterning modulation can also be controlled. A typical example of patterning with a seesaw field modulation is presented in Figure 5a,b.

The transmitted intensity $I(x)$ varies along the x-axis, parallel to the capillary axis and along the direction of mask displacement, confirming the expected asymmetric triangular profile of the phase shift of the pattern. Indeed, the local phase shift, $\Delta L(x) \approx [I(x)]^{1/2}$, (Figure 5c) follows the general shape of the field. The phase modulation of the material can also be conveniently visualized by inserting a Berek optical compensator in the light path, contributing a negative position-dependent phase shift, $\Delta Lc(x,y)$. In first approximation, $\Delta Lc(x,y)$ is independent of x and increases linearly with y. The addition of $\Delta Lc(x,y)$ and $\Delta L(x)$ results in the interference image shown in Figure 5b. The black bands correspond to the regions where the two phase-shifts compensate, $\Delta Lc(x,y) + \Delta L(x) = 0$. In the absence of modulation, a single horizontal black band would be observed. Due to the modulation, the black band deforms, generating striations that follow the same $\Delta L(x)$ dependence as that deduced from the intensity profile (Figure 5c). It must be emphasized that $\Delta L(x)$ obtained in this way is a direct result,

dx.doi.org/10.1021/am300980r | ACS Appl. Mater. Interfaces 2012, 4, 4296−4301

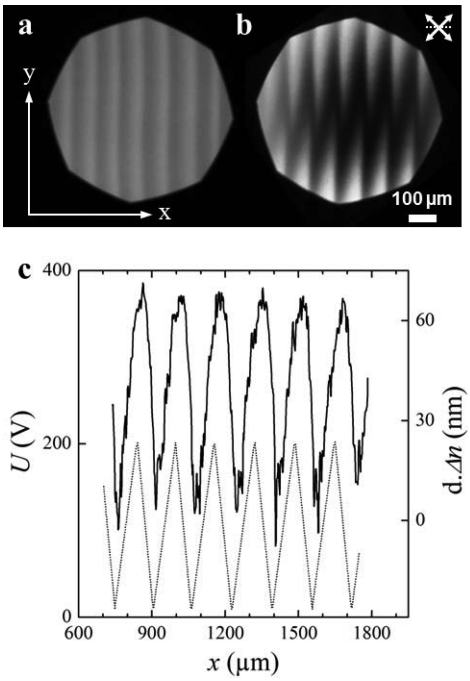

Figure 5. (a) POM image of a composite sample (ϕ = 0.4%) patterned with a seesaw modulation. (b) The same as (a) recorded with a Berek compensator inserted at 45° (dotted line). (c) Corresponding applied a.c. voltage amplitude at the position of the traveling polymerization front (dotted line) and phase-shift measured after polymerization (continuous line).

independent of the spatial variation of light intensity in the microscope field of view and other artifacts.

Finally, we now compare our alignment process with the other field-alignment methods of clay-based hybrid materials previously published, such as refs 18 and 19. The hybrid materials described in this work are hydrogels, whereas previous studies deal with epoxy or polypropylene matrices. The latter always require an organophilic treatment of the clay platelets which can be dispensed with for hydrogels. The volume fractions of the materials described here are of order of 0.3%, which is much lower than those (~3%) of the previously published materials. Consequently, the viscosity of the doped starting suspensions is quite low, which allows us to use low-intensity electric fields and to modulate alignment while polymerization proceeds. However, one drawback of our approach is the onset of physical gelation at volume fractions ~1% beyond which no effect of the electric field was observed. Another striking difference between the materials described here and those published in literature lies in the influence of temperature. Indeed, the former ones, being generally considered as "hard-particle" suspensions, are little sensitive to temperature, whereas the latter ones are polymerized by heating. In contrast, our polymerization process is based on photocross-linking, which actually provides a very convenient tool to pattern platelet orientation at will.

4. CONCLUSION

We have shown here that aqueous suspensions of natural swelling clays can be used to produce novel clay−polymer nanocomposites in which clay platelets are perfectly exfoliated. Moreover, these hydrogels are stiff enough to keep the shape of the vials in which they were molded. Actually, preliminary rheological experiments showed that their G' elastic modulus is on the order of 1×10^5 Pa. Furthermore, we were able to control platelet orientation within the polymer matrix by applying high-frequency a.c. electric fields. Our simple polymerization procedure allows patterning platelet orientation, at length scales down to 20 μm. Such patterned materials could find applications as thin-film passive optical elements, e.g. phase gratings with controlled profile (step-like, seesaw, ...) of the local phase delay. However, our samples are presently a few millimeters in size and, although this process could in principle easily be extended to centimetric samples, further efforts are needed in order to scale it up to even larger sample sizes useful for industrial purposes. This straightforward technique can be easily extended to other natural or synthetic inorganic anisotropic nanoparticles that form stable dispersions.[28−32] Indeed, nanocomposites filled with other natural swelling clay minerals such as nontronite and montmorillonite could also be patterned.[33] The modulation of clay particle orientation over the 1 μm to 1 mm length scale could be employed to produce diffraction gratings for electromagnetic waves in the Infrared domain and for ultrasounds. Because our technique is quite versatile, other suspensions of mineral nanosheets, better suited to specific applications, could easily be used. Ultimately, these gratings could be used to engineer photonic (IR) and phononic crystals.

AUTHOR INFORMATION

Corresponding Author

*E-mail: erwan-nicolas.paineau@u-psud.fr.

Present Address

[⊥]CEREGE, UMR 6635, Aix Marseille University, 13545 Aix en Provence cedex 4, France

Notes

The authors declare no competing financial interest.

ACKNOWLEDGMENTS

This work was funded by the French ANR agency (Agence Nationale de la Recherche, programme blanc ANISO). I.D. acknowledges financial support from Institut National Polytechnique de Lorraine (Nancy).

REFERENCES

(1) Kojima, Y.; Usuki, A.; Kawasumi, M.; Okada, A.; Fukushima, Y.; Kurauchi, T.; Kamigaito, O. *J. Mater. Res.* **1993**, *8*, 1185−1189.
(2) Giannelis, E. P. *Adv. Mater.* **1996**, *8*, 29−35.
(3) LeBaron, P. C.; Wang, Z.; Pinnavaia, T. J. *Appl. Clay Sci.* **1999**, *15*, 11−29.
(4) Sinha Ray, S.; Okamoto, M. *Prog. Polym. Sci.* **2003**, *28*, 1539−1641.
(5) Bitinis, N.; Hernandez, M.; Verdejo, R.; Kenny, J. M.; Lopez-Manchado, M. A. *Adv. Mater.* **2011**, *23*, 5229−5236.
(6) Lan, T.; Kaviratna, P. D.; Pinnavaia, T. J. *Chem. Mater.* **1994**, *6*, 573−575.
(7) Triantafyllidis, K. S.; LeBaron, P. C.; Park, I.; Pinnavaia, T. J. *Chem. Mater.* **2006**, *18*, 4393−4398.
(8) (a) Haraguchi, K.; Takehisa, T. *Adv. Mater.* **2002**, *14*, 1120−1124. (b) Haraguchi, K.; Ebato, M.; Takehisa, T. *Adv. Mater.* **2006**, *18*, 2250−2254. (c) Haraguchi, K. *Colloid Polym. Sci.* **2011**, *289*, 455−473 and references therein..
(9) Ebina, T.; Mizukami, F. *Adv. Mater.* **2007**, *19*, 2450−2453.
(10) Wang, Q.; Mynar, J. L.; Yoshida, M.; Lee, E.; Lee, M.; Okuro, K.; Kinbara, K.; Aida, T. *Nature* **2010**, *463*, 339−343.
(11) Schmidt, G.; Nakatani, A. I.; Butler, P. D.; Han, C. C. *Macromolecules* **2002**, *35*, 4725−4732.

(12) Shibayama, M.; Karino, T.; Miyazaki, S.; Okabe, S.; Takehisa, T.; Haraguchi, K. *Macromolecules* **2005**, *38*, 10772−10781.
(13) Okamoto, M.; Nam, P. H.; Maiti, P.; Kotaka, T.; Hasegawa, N.; Usuki, A. *Nano Lett.* **2001**, *1*, 295−298.
(14) Murata, K.; Haraguchi, K. *J. Mater. Chem.* **2007**, *17*, 3385−3388.
(15) Vaia, R. A.; Cindi, L. D.; Natarajan, L. V.; Tondiglia, V. P.; Tomlin, D. W.; Bunning, T. J. *Adv. Mater.* **2001**, *13*, 1570−1574.
(16) De Gennes, P. G. *The Physics of Liquid Crystals*; Clarendon: Oxford, U.K., 1979.
(17) Commeinhes, X.; Davidson, P.; Bourgaux, C.; Livage, J. *Adv. Mater.* **1997**, *9*, 900−903.
(18) (a) Koerner, H.; Jacobs, D.; Tomlin, D. W.; Busbee, J. D.; Vaia, R. D. *Adv. Mater.* **2004**, *16*, 297−302. (b) Koerner, H.; Hampton, E.; Dean, D.; Turgut, Z.; Drummy, L.; Mirau, P.; Vaia, R. *Chem. Mater.* **2005**, *17*, 1990−1996.
(19) (a) Park, J. U.; Choi, Y. S.; Cho, K. S.; Kim, D. H.; Ahn, K. H.; Lee, S. J. *Polymer* **2006**, *47*, 5145−5153. (b) Kim, D. H.; Cho, K. S.; Mitsumata, T.; Ahn, K. H.; Lee, S. J. *Polymer* **2006**, *47*, 5938−5945.
(20) Paineau, E.; Antonova, K.; Baravian, C.; Bihannic, I.; David-son, P.; Dozov, I.; Impéror-Clerc, M.; Levitz, P.; Madsen, A.; Meneau, F.; Michot, L. J. *J. Phys. Chem. B* **2009**, *113*, 15858−15869.
(21) Paineau, E.; Bihannic, I.; Baravian, C.; Philippe, A. M.; Davidson, P.; Levitz, P.; Funari, S. S.; Rochas, C.; Michot, L. J. *Langmuir* **2011**, *27*, 5562−5573.
(22) Dozov, I.; Paineau, E.; Davidson, P.; Antonova, K.; Baravian, C.; Bihannic, I.; Michot, L. J. *J. Phys. Chem. B* **2011**, *115*, 7751−7765.
(23) Post, J. L.; Cupp, B. L.; Madsen, F. T. *Clays Clay Miner.* **1997**, *45*, 240−250.
(24) Belamie, E.; Davidson, P.; Giraud-Guille, M. M. *J. Phys. Chem. B* **2004**, *108*, 14991−15000.
(25) Paineau, E.; Michot, L. J.; Bihannic, I.; Baravian, C. *Langmuir* **2011**, *27*, 7806−7819.
(26) Lu, C.; Mai, Y. W. *Compos. Sci. Technol.* **2007**, *67*, 2895−2902.
(27) Alix, S.; Follain, N.; Tenn, N.; Alexandre, B.; Bourbigot, S.; Soulestin, J.; Marais, S. *J. Phys. Chem. C* **2012**, *116*, 4937−4947.
(28) Sasaki, T.; Watanabe, M.; Hashizume, H.; Yamada, H.; Nakazawa, H. *J. Am. Chem. Soc.* **1996**, *118*, 8329−8335.
(29) Schaak, R. E.; Mallouk, T. E. *Chem. Mater.* **2000**, *12*, 3427−3434.
(30) Gabriel, J. C. P.; Camerel, F.; Lemaire, B. J.; Desvaux, H.; Davidson, P.; Batail, P. *Nature* **2001**, *413*, 504−508.
(31) van der Beek, D.; Davidson, P.; Wensink, H. H.; Vroege, G. J.; Lekkerkerker, H. N. W. *Phys. Rev. E* **2008**, *77*, 031708.
(32) (a) Miyamoto, N.; Iijima, H.; Ohkubo, H.; Yamauchi, Y. *Chem. Commun.* **2010**, *46*, 4166−4168. (b) Nakato, T.; Nakamura, K.; Shimada, Y.; Shido, Y.; Houryu, T.; Iimura, Y.; Miyata, H. *J. Phys. Chem. C* **2010**, *114*, 8934−8939.
(33) Michot, L. J.; Bihannic, I.; Maddi, S.; Funari, S. S.; Baravian, C.; Levitz, P.; Davidson, P. *Proc. Natl. Acad. Sci. U.S.A.* **2006**, *44*, 16101−16104.